Ultrasonics Sonochemistry 92 (2023) 106244

Contents lists available at ScienceDirect

Ultrasonics Sonochemistry

journal homepage: www.elsevier.com/locate/ultson

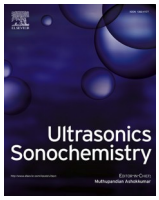

Microstructure evolution and grain refinement of ultrasonic-assisted soldering joint by using Ni foam reinforced Sn composite solder

Huang He [a,b], Lizhi Song [b], Haitao Gao [c], Yong Xiao [b,*], Yi Cao [d,*]

[a] College of Mechanical and Electrical Engineering, Hubei Three Gorges Polytechnic, Yichang 443000, China
[b] School of Materials Science and Engineering, Wuhan University of Technology, Wuhan 430070, China
[c] China-Ukraine Institute of Welding, Guangdong Academy of Sciences, Guangzhou 510650, China
[d] Institute for Advanced Materials, Hubei Normal University, Huangshi 435002, China

ARTICLE INFO

Keywords:
Ni foam
Composite solder
Ultrasonic-assisted soldering
Foam porosity
Grain refinement

ABSTRACT

In this investigation, ultrasonic-assisted soldering at 260 °C in air produced high strength and high melting point Cu connections in 60 s using Ni foam reinforced Sn composite solder. Systematically examined were the microstructure, grain morphology, and shear strength of connections made with various porosities of Ni foam composite solders. Results shown that Ni foams as strengthening phases could reinforce Sn solder effectively. The addition of Ni foam accelerated the metallurgical reaction due to great amount of liquid/solid interfaces, and refined the intermetallic compounds (IMCs) grains by ultrasonic cavitation. The joints had different IMCs by using Ni foam with different porosity. Layered $(Cu,Ni)_6Sn_5$ and $(Ni,Cu)_3Sn_4$ phases both existed in Cu/Ni60-Sn/Cu joint while only $(Cu,Ni)_6Sn_5$ IMCs grew in Cu/Ni98-Sn/Cu joint. As ultrasonic time increasing, Ni skeletons were dissolved and the IMCs were peeled off from substrates and broken into small particles. And then, the IMCs gradually dissociated into refined particles and distributed homogeneously in the whole soldering seam under cavitation effects. Herein, the Cu/Ni60-Sn/Cu joint ultrasonically soldered for 60 s exhibited the highest shear strength of 86.9 MPa, as well as a high melting point about 800 ℃ for the solder seam composed of Ni skeletons and Ni-Cu-Sn IMCs. The characterization indicated that the shearing failure mainly occurred in the interlayer of the soldering seam. The homogeneous distributed granular IMCs and Ni skeletons hindered the crack propagation and improved the strength of Cu alloy joints.

1. Introduction

Excellent mechanical qualities and high melting-point Cu interconnects are required to ensure the electronic device dependability because of the fast growth of downsizing and functional integration in components [1,2]. It is becoming necessary for an increasing number of electronic components to be able to function under harsh conditions, such as those involving high temperatures and high strength. For instance, some power devices made of silicon carbide (SiC) and gallium nitride (GaN) could operate at a temperature up to 600 °C [3,4]. The conventional *sn*-based solder, however, falls short of those specifications in several respects. In order to produce Cu joints with high strength and high serves temperature, while soldered at low temperature in a short time, it is crucial to create new lead-free *sn*-based solders and packaging techniques [5].

Our current research included fabricating and using Ni foam reinforced Sn composite solder foils to solder Cu alloy and Al alloy, and it revealed that the use of Ni-skeletons and Ni-Sn reactants significantly increased the strengths of joint [6,7]. The analysis results show that continuous reticular structure inhibits the aggregation of the reinforcing phase and improves the combination between Sn solder and reinforcing phases [8]. Moreover, the Ni atoms refine the intermetallic compounds (IMCs) grains of Cu joints during soldering. Thus, the reticular Ni foam has been proven as an excellent reinforcing structure to obtain high strength of joints.

The packaging technique, in addition to *sn*-based solders, is also important. A quick and effective way to create junctions with a high melting point at low temperatures is to use ultrasonic-assisted soldering [9,10]. According to previous research, ultrasonic-assisted soldering can accelerate metallurgic reaction and form fully IMCs joints in Ni-Sn system [11,12]. The cavitation and acoustic streaming caused by ultrasonic waves during the soldering process provide a localized environment

* Corresponding authors.
E-mail addresses: yongxiao@whut.edu.cn (Y. Xiao), caoyi@hbnu.edu.cn (Y. Cao).

https://doi.org/10.1016/j.ultsonch.2022.106244
Received 16 September 2022; Received in revised form 16 November 2022; Accepted 25 November 2022
Available online 2 December 2022

with very high pressure and temperature, which encourages wetting and speeds up the metallurgical reaction [13–15]. Furthermore, acoustic cavitation microbubbles mainly occurred at the interfaces of liquid/solid under cavitation effect [16–18]. During the ultrasonic-assisted soldering, the Ni foam creates additional liquid/solid interfaces for the formation of acoustic cavitation microbubbles, which speeds up the diffusion of Cu, Ni, and Sn and encourages the reaction. Additionally, the reaction rate with various Ni particle amounts is obviously different, which has been shown to be an efficient grain refiner for boosting the shear strength of the Cu-Sn wafer bonding joints [19–21]. Hence, high strength and high melting-point Cu joints can be achieved in a short time by ultrasonic assisted soldering [11,22].

Following the example above, various porosities of Ni foam reinforced Sn composite solder foils were made, and Cu connections were effectively constructed using ultrasonic-assisted soldering at 260 °C. Additionally, it was extensively examined how the microstructure and shear strength of Cu joints were affected by the foam porosities and the duration of the ultrasonic vibration. Moreover, the mechanism of efficient metallurgical bonding and refined microstructure was focused on. In this study, dependable Cu joints with exceptional strength and a high melting point were obtained quickly at a low temperature. These joints have a bright future for use in the packaging of high-power devices.

2. Experimental materials and methods

The soldering substrate was commercial T2-Cu alloy with a size of $10 \times 20 \times 3$ mm^3. Two kinds of Ni foam foils with 98 % and 60 % porosities and a thickness of 0.5 mm were employed as the strengthening phase to reinforce Sn solder. Fig. 1 shows the 3D super depth optical micrographs of Ni foams. As the open-cell Ni foams exhibited three-dimensional continuous reticular structures, the Ni skeletons were continuous, interlaced and twisted together. The Ni foam with 60 % porosity was relatively more crowded than that with 98 % porosity. The average pore diameter of Ni foams with porosities of 98 % and 60 % were 200 μm and 50 μm, respectively.

The schematic diagram of the Ni-Sn composite solder manufacturing process and ultrasonic-assisted soldering method is shown in Fig. 2. Ni foams were placed into a molten Sn bath at 260 °C for 10 s to fully fill with Sn solder, and then the bath was removed. Vacuum was used during the preparation process to reduce voids in the composite solder. Ni foam/Sn composite solders with porosities of 98 % and 60 %, referred to as Ni98-Sn and Ni60-Sn, respectively, were developed. The composite solder foils were rolled to 220 μm and then cut into 10×10 mm^2 before soldering. As shown in Fig. 2, the soldering system was set in a self-made clamping apparatus with the composite solder foil placed between two Cu substrates with an overlapping area of 10×10 mm^2. In the soldering process, placed the TC4 Ti alloy ultrasonic vibration rod with a tip diameter of Ø3 mm vertically in the center of the upper Cu substrate. An ultrasonic machine (KESON KX-800) worked at 30 kHz and the soldering gap was fixed at 150 μm during the soldering process. Both the pressure and the power of the ultrasonic vibration were held constant at 0.2 MPa and 350 W, respectively. We made use of a heating unit, and a K-type thermocouple was used to monitor and regulate the temperature at which the soldering was performed. Before beginning the soldering process, all of the surfaces of the copper substrates and the composite solder foils were ground and then ultrasonically cleaned in ethanol. The temperature of the soldering was 260 ℃, the ultrasonic vibration was put on for five seconds, ten seconds, twenty seconds, thirty seconds and it lasted for sixty seconds, respectively. The sample of ultrasonic soldering was brought down to room temperature while being cooled at ambient temperature and under pressure.

The samples of soldering were first coated with epoxy, then manually ground with papers containing grades 180, 400, 600, 1200 and 2000 silicon carbide, and then polished with a diamond polishing agent measuring 1 mm in diameter. Analyses of the microstructure and phase composition of soldering joint were carried out with the assistance of an energy dispersive X-ray spectrometer (EDS, INCAX-ACT), a scanning electron microscope (SEM, FEI Quanta 450), and an electron probe micro-analyzer (EPMA, JXA-8230). The soldering Cu joints were cut into a size of Φ3 × 5 mm to determination the corresponding melting-point and phase transition temperature by the differential scanning calorimetry (DSC) detector with a heating rate of 30 ℃/min. A scanning electron microscope that was outfitted with an electron back scatter diffraction analyzer (SEM/EBSD, JSM-7001F) was utilized in order to measure the phase distribution and grain mapping of ultrasonically soldered Cu joint. This was accomplished by using the SEM instrument.

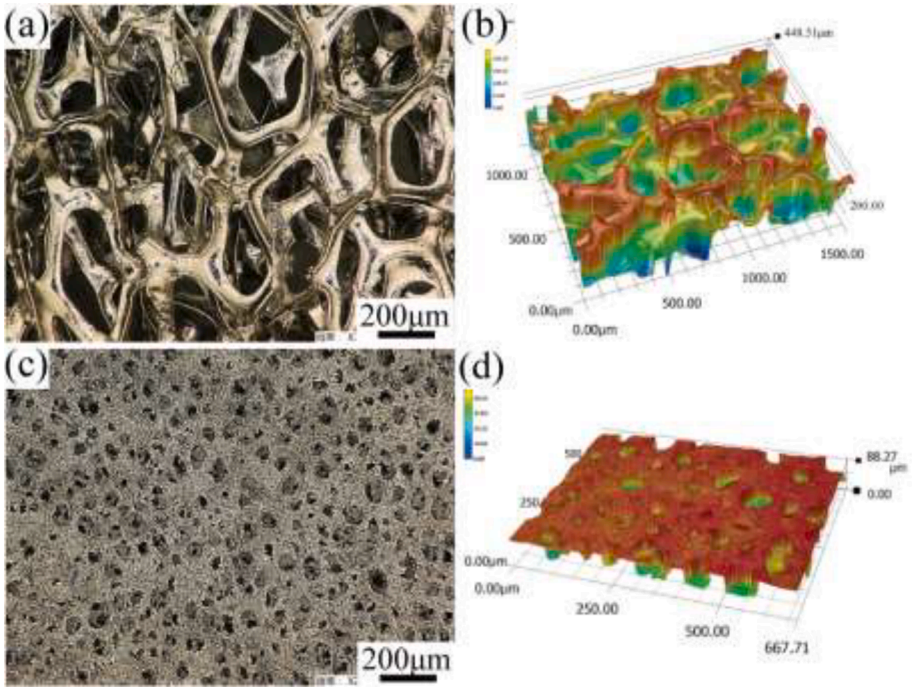

Fig. 1. 3D Super Depth Digital micrographs of Ni-foams with different porosity. (a) (b) 98% porosity, (c) (d) 60% porosity.

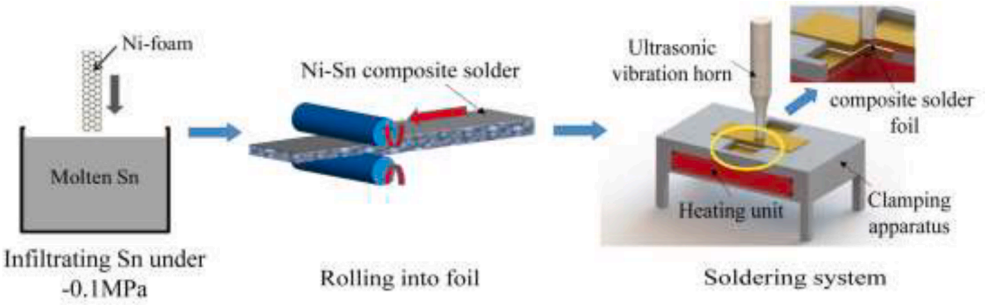

Fig. 2. Schematic diagram of the manufacture of Ni-Sn composite solder and ultrasonic soldering process.

The tensile strength of pure Sn solder, different porosity Ni foams, the corresponding composite solder foils and the shear strength of soldering joints, were evaluated with the assistance of an electron tension testing equipment (Instron-5569). A diagrammatic sketch of the clamping apparatus that was employed in this investigation can be found in our prior studies [23]. The shear strain rate was set at 0.5 mm/min. An average shear strength was calculated by using five samples for each parameter.

3. Results and discussion

3.1. Microstructure and strength of Ni-Sn composite solders

In Fig. 3, composite solder foils made of Ni98-Sn and Ni60-Sn are shown in cross-section. Ni skeletons and Sn matrix, respectively, are represented by the dark and white phases. Without any holes or other flaws, pure Sn solder entirely fills the empty area in the Ni foam. The Ni skeleton fraction of Ni60-Sn foil is much larger than that of Ni98-Sn foil when comparing Fig. 3(a) and 3(c). On Ni skeleton surfaces, there are few reactants. Some small particles adhered to the Ni skeleton surface and is becomes rough as can be shown in Fig. 3(b) and a gray serrate reaction layer is formed in Fig. 3(d). In this research, the Ni skeleton maintains a three-dimensional continuous network structure and is distributed randomly in Sn solder, giving the Ni-Sn composite solder an interpenetrating reinforcing structure.

The results of a test to determine the tensile strength of pure Sn, Ni98-Sn, and Ni60-Sn foils are shown in Fig. 4. Tensile strengths of pure

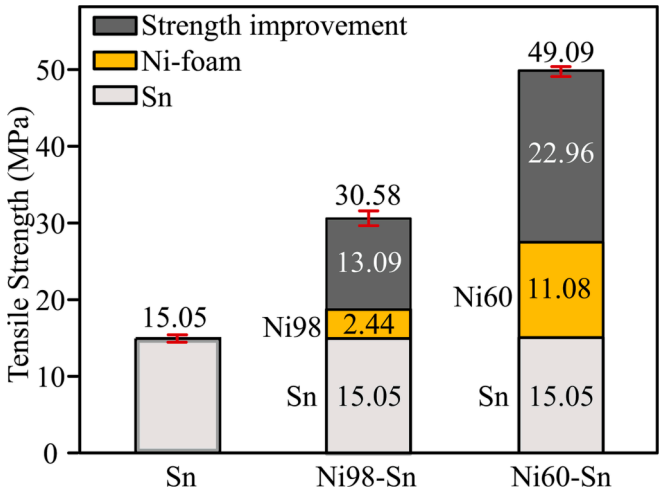

Fig. 4. Tensile strength of pure Sn, Ni98-Sn and Ni60-Sn solder foils.

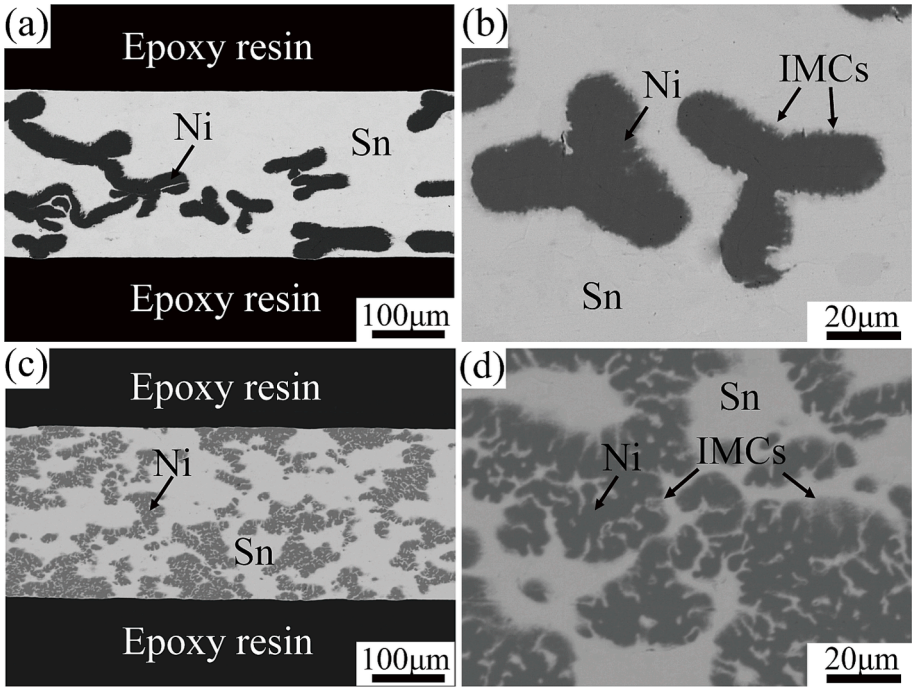

Fig. 3. Cross-section images of (a) (b) Ni98-Sn and (c) (d) Ni60-Sn composite solder foils.

Sn solder foil, 98 % porosity's Ni foam and 60 % porosity's Ni foam are 15.53 MPa, 2.44 MPa and 11.08 MPa, respectively. The sum strengths are 13.09 MPa and 22.96 MPa lower than those of Ni98-Sn and Ni60-Sn solder foils respectively, at 30.58 MPa and 49.09 MPa. As a result, the sum tensile strength of the Sn matrix and matching Ni foam reinforcement is lower than that of Ni-Sn composite solders with varying porosities. This is primarily attributable to the Ni foam skeleton's interpenetrating structure and continuous spatial distribution, which not only preserve their individual mechanical qualities but also fortify the whole composite solder. Ni foam thus efficiently reinforces *sn*-based composite solder when used as a strengthening structure.

3.2. Microstructure and grain of Cu/Ni-Sn/Cu joints

The Cu joints employing Ni98-Sn foils that were ultrasonically soldered for 5 s, 30 s, and 60 s are shown in cross-sectional pictures in Fig. 5. The Ni skeletons are firmly compressed and attached, and some scattered gray particles are growing around the Ni skeleton. Additionally, when Cu substrates are ultrasonically soldered for 5 s, continuous reaction layers are created on their surfaces, as can be seen in Fig. 5(a). The enlarged picture of the soldering seam interface in Fig. 5(b) indicates a reaction layer of Cu interface with a fluctuating average thickness of 1.7 μm. However, Cu substrate interface is not very flat, a small bump even appears in some areas. The irregular IMCs particles have different sizes, and a few reveal obvious cracks. Some IMCs particles tend to break away from Ni skeleton and Cu substrate.

Fig. 5(c)-(d) show the cross-section of Cu/Ni98-Sn/Cu joint that was ultrasonically soldered for 30 s. The number of granular IMCs formed around the Ni skeleton and the number of microscopic IMCs particles in the Sn matrix greatly increase when compared to the joint soldered for 5 s. The Ni skeleton surface exhibits a very thin IMCs layer with no obvious granular IMCs, which indicates that primeval granular IMCs have been stripped off the Ni skeleton. The cracks on both large and part small particles also prove the spalling phenomenon. Fig. 5(d) shows that the interfaces of Cu substrates are no longer flat, and the thickness of IMCs layer is 2.2 μm. Besides, the IMCs begin to extend into the Cu substrates, and even the local Cu substrate appears as an island suspended in the reaction layer.

Fig. 5(e)-(f) exhibit the cross-section images of Cu/Ni98-Sn/Cu joint ultrasonically soldered for 60 s. Under this condition, the IMCs particles are uniformly distributed in the entire soldering seam, as well as the IMCs layer of Cu interface becomes obviously thicker, significantly increased to 5.1 μm. With the obvious dissolution of Ni skeleton, the Cu substrate surface fluctuation grows greatly, gradually showing a jagged shape (Fig. 5(e)). Furthermore, the thickness of Ni skeleton is significantly decreased and the partial dissolution is very serious. The majority of IMCs particles spall off from the skeleton with a granular shape. The size of IMCs particles is inconsistent in the seam, and cracks appear in the larger particles, indicating that these particles will become smaller.

Table 1 displays the findings of the EDS analysis and the phase constitutions of the locations indicated in Fig. 5. The findings show that (Ni + Cu) has an atomic ratio of around 6:5 to Sn. Considering prior

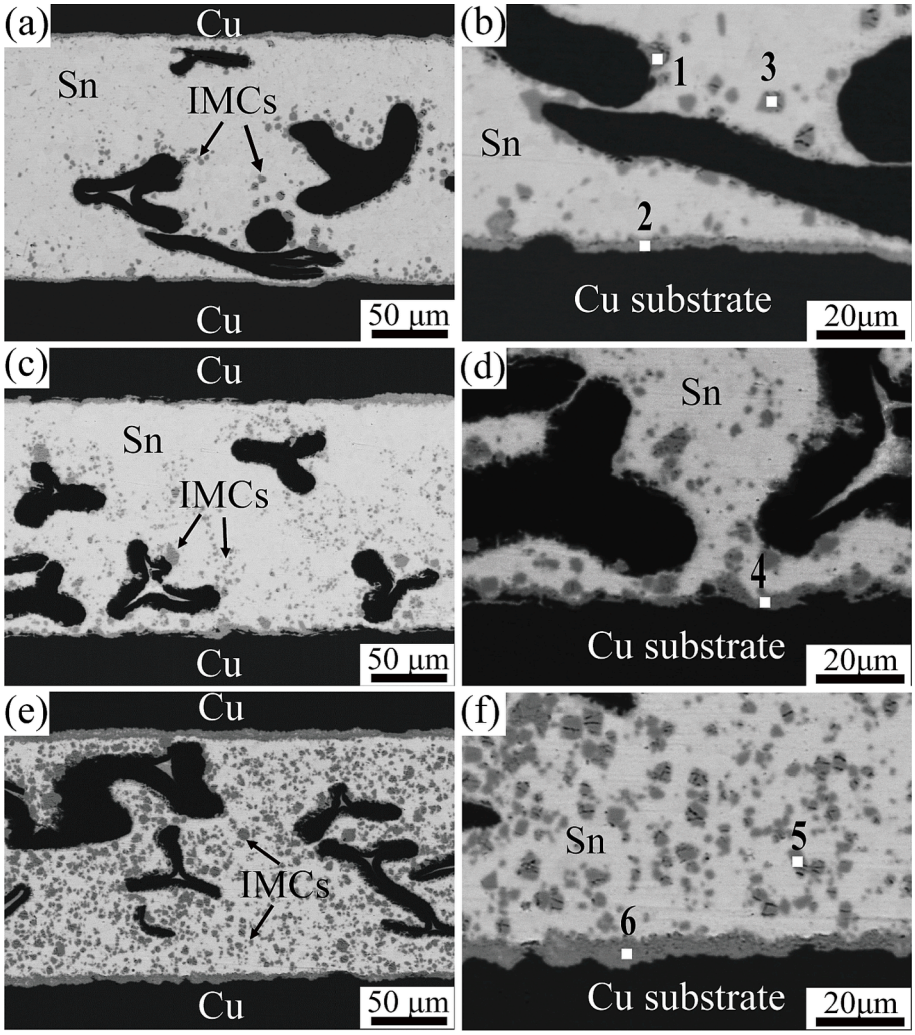

Fig. 5. Cross-section images of Cu/Ni98-Sn/Cu joints ultrasonically soldered for (a) (b) 5 s, (c) (d) 30 s, (e) (f) 60 s.

Table 1
Element compositions of regions marked in Fig. 5.

Spots	Soldering time (s)	Element composition (at. %)			Phase
		Sn	Ni	Cu	
1	5	48.32	20.40	31.28	$(Cu,Ni)_6Sn_5$
2	5	46.20	6.14	47.66	$(Cu,Ni)_6Sn_5$
3	5	49.08	12.41	38.51	$(Cu,Ni)_6Sn_5$
4	30	50.54	6.75	42.71	$(Cu,Ni)_6Sn_5$
5	60	48.45	10.81	40.74	$(Cu,Ni)_6Sn_5$
6	60	49.64	5.61	44.75	$(Cu,Ni)_6Sn_5$

research [20], the gray particles marked by "1″ to "6" are deduced to be $(Cu,Ni)_6Sn_5$ phase. Thus, the IMCs of Sn/Cu and Sn/Ni interfaces are both $(Cu,Ni)_6Sn_5$. In addition, comparing regions marked by "1" and "3", the Cu and Ni content of $(Cu,Ni)_6Sn_5$ around Ni skeleton are different from that next to Cu substrates. The changes indicate that the Cu atoms in $(Cu,Ni)_6Sn_5$ have been partially replaced by Ni atoms.

The microstructures and morphologies of Cu joints vary greatly using different composite solders, owing to the different volume fraction of Ni skeleton between Ni98-Sn foil and Ni60-Sn foil. Fig. 6 shows the cross-section images of Cu/Ni60-Sn/Cu joint ultrasonically soldered for 5 s, 30 s and 60 s. As shown in Fig. 6(a)-(b), a large amount of Sn remains and the Ni skeletons are in large blocks with a local deposited shape in the soldering seam when ultrasonically soldered for 5 s. Because the continuous reaction layers are formed on Cu substrates and Ni skeleton surfaces, a small number of IMCs particles exist at the edge of the blocky Ni skeleton. Fig. 6(c)-(d) present the cross-section images of Cu joint ultrasonically soldered for 30 s. As the IMCs grow significantly with obvious decrease of the residual Sn, the dissolution of Ni foam is relatively obvious, and part of Ni skeletons are mixed in the blocks as fine threads. The IMCs at the substrate interfaces show relatively uniform continuous layers. A great amount of granular IMCs appears around the Ni skeleton, which is very fine and uniform in size. Fig. 6(e)-(f) exhibit the cross-section images of Cu joint ultrasonically soldered for 60 s. As shown in Fig. 6(e)-(f), the joint has no residual Sn and the Ni foam also dissolves seriously, and the originally locally agglomerated Ni skeleton disappears, while only some small filamentous or lumpy residues remain in the joint. The thicknesses of reaction layers on two sides of Cu substrate interfaces are the same and the flatness of the upper and lower substrates tends to be the same.

The findings of the EDS analysis and the phase constitutions of the locations indicated in Fig. 6 are shown in Table 2. The findings of the EDS study indicate that the uniform continuous layer around the Ni skeletons is $(Ni,Cu)_3Sn_4$ phase (spot 1 and 3) and that at Cu substrate interface is $(Cu,Ni)_6Sn_5$ IMCs (spot 2, 5, and 6). The joint has a little residual Sn when ultrasonically soldered for 30 s (spot 4). Analyzing and comparing the element composition in $(Cu,Ni)_6Sn_5$, the contents of Cu and Ni are still related to their position, the Cu content of $(Cu,Ni)_6Sn_5$ near the Cu substrate is higher, while the Ni content near the Ni skeletons side is higher.

The phase distribution and grain morphology of Cu joints that were

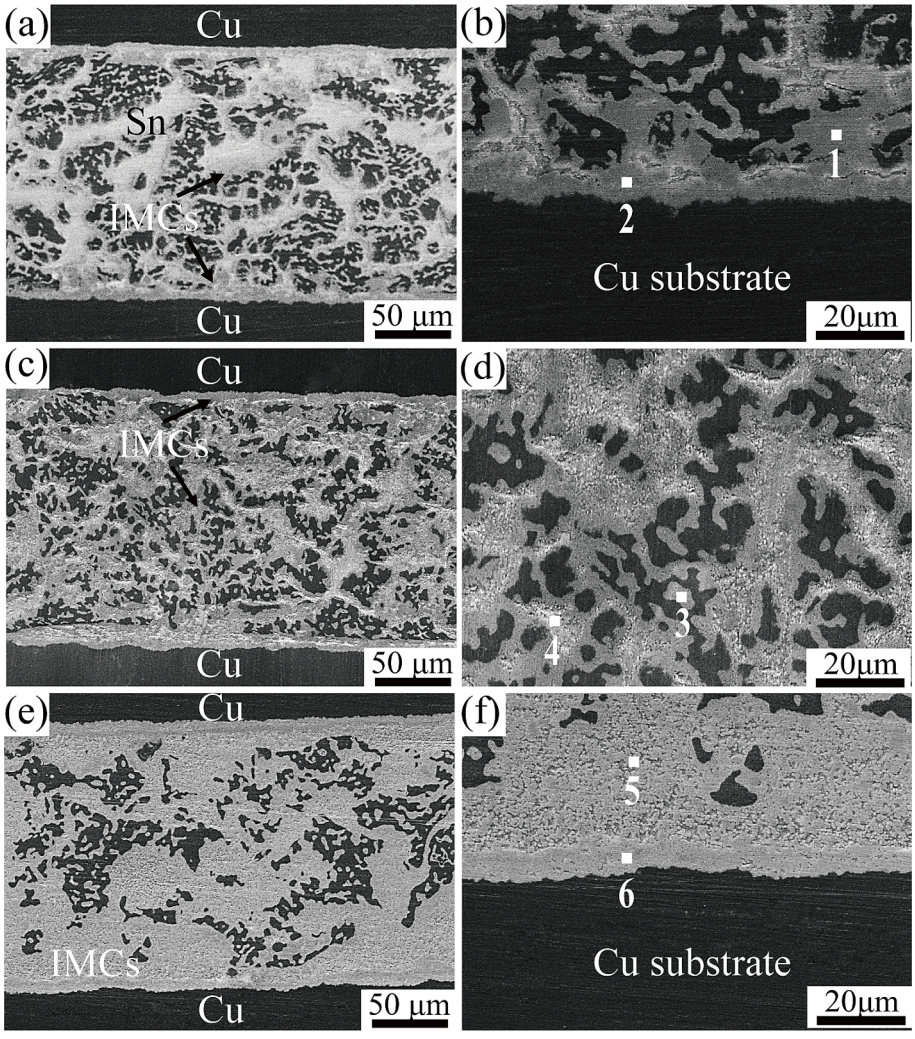

Fig. 6. Cross-section images of Cu/Ni60-Sn/Cu joints ultrasonically soldered for (a) (b) 5 s, (c) (d) 30 s, (e) (f) 60 s.

Table 2
Element compositions of regions marked in Fig. 6.

Spots	Soldering time (s)	Element composition (at. %)			Phase
		Sn	Ni	Cu	
1	5	49.49	12.26	38.25	$(Cu,Ni)_6Sn_5$
2	5	49.97	4.41	45.62	$(Cu,Ni)_6Sn_5$
3	30	58.36	24.39	17.25	$(Ni,Cu)_3Sn_4$
4	30	100.0	0	0	Sn
5	60	49.96	7.50	42.54	$(Cu,Ni)_6Sn_5$
6	60	47.90	4.65	47.45	$(Cu,Ni)_6Sn_5$

ultrasonically soldered with various Ni-Sn composite solders were examined using an EBSD detector. Cu/Ni98-Sn/Cu joints' phase and grain mapping are shown in Fig. 7. On the surfaces of Cu and Ni, the $(Cu,Ni)_6Sn_5$ phases arise without the presence of any Ni-Sn reactants. The junction is mostly made up of blocky β-Sn phase, as presented in Fig. 7 (a)-(b), although a thin $(Cu,Ni)_6Sn_5$ IMC layer forms on the Cu substrate surface after the connection has been soldered for 5 s. The quick growing of $(Cu,Ni)_6Sn_5$ phase at Cu substrate contacts proves that Ni-Sn composite solders were used to achieve the superior metallurgical reaction during ultrasonic vibration. These findings agree with those from the aforementioned SEM and EDS research. The IMCs separate from Cu substrates and Ni skeletons, which dissociate to minute particles in the soldering seam under cavitation action and constant mechanical vibration. As illustrated in Fig. 7(c)-(d), the $(Cu,Ni)_6Sn_5$ phase dissociates into tiny particles with an average grain size of around 5.8 μm when the soldering duration is raised to 60 s.

The phase mapping and grain mapping of the Cu/Ni60-Sn/Cu joints are shown in Fig. 8. In Fig. 8(a)-(b), in addition to the Ni skeletons and the Sn matrix, the IMCs dominate in the seam that was soldered for 5 s. These IMCs are mostly constituted of the $(Cu,Ni)_6Sn_5$ and $(Ni,Cu)_3Sn_4$ phases. However, the $(Cu,Ni)_6Sn_5$ phase is produced on Cu substrate interfaces, and there is only a very small layer of $(Ni,Cu)_3Sn_4$ on the surface of the Ni skeleton. Fig. 8(c)-(d) present that the remained *sn*-rich solder are exhausted and the $(Cu,Ni)_6Sn_5$ and $(Ni,Cu)_3Sn_4$ phases are increased. As the soldering time prolongs, the Ni skeleton is gradually dissolved and the granular IMCs gradually increase and finally uniformly distribute throughout the whole soldering seam. When ultrasonic-assisted soldering time is increased from 5 s to 60 s, the interfacial reaction layer transitions from a compact $(Ni,Cu)_3Sn_4$ IMC layer to a loose IMC layer, as seen in Fig. 8. The Ni foam skeletons are also substantially dissolved. Only a very thin $(Ni,Cu)_3Sn_4$ layer is present on the surface of the Ni skeleton, despite the fact that the $(Cu,Ni)_6Sn_5$ phase is dispersed throughout the joint. The IMCs are equally distributed across the seam and subsequently become fine particles with an average grain size of 4.5 μm to 0.6 μm.

3.3. Metallurgic bonding mechanism of joint

The excellent metallurgic reaction occurred by using Ni-Sn composite solders under ultrasonic vibration. Generally, the ultrasonic-assisted soldering promotes the diffusion of atoms and increases the reaction rate with Sn through acoustic cavitation effects [15]. On the one hand, the collapse of acoustic cavities induces micro-jets and shockwaves, which leads to high temperature and pressure in the liquid Sn [11,16,24]. When cavitation bubbles burst at the solid/liquid interface, it can directly melt Cu and Ni and induce local supersaturated dissolution [25]. On the other hand, the cavitation bubble blasting usually affects 200 nm surrounding [26], which means that the heat generated by the "hot spot" will quickly form a temperature gradient in the surrounding area [27,28]. The differential in temperature encourages atom diffusion and grain development. According to widespread consensus [29], the Ni_3Sn_4 layer at the Ni/Sn interface serves as a diffusion barrier layer, but the presence of a temperature gradient may

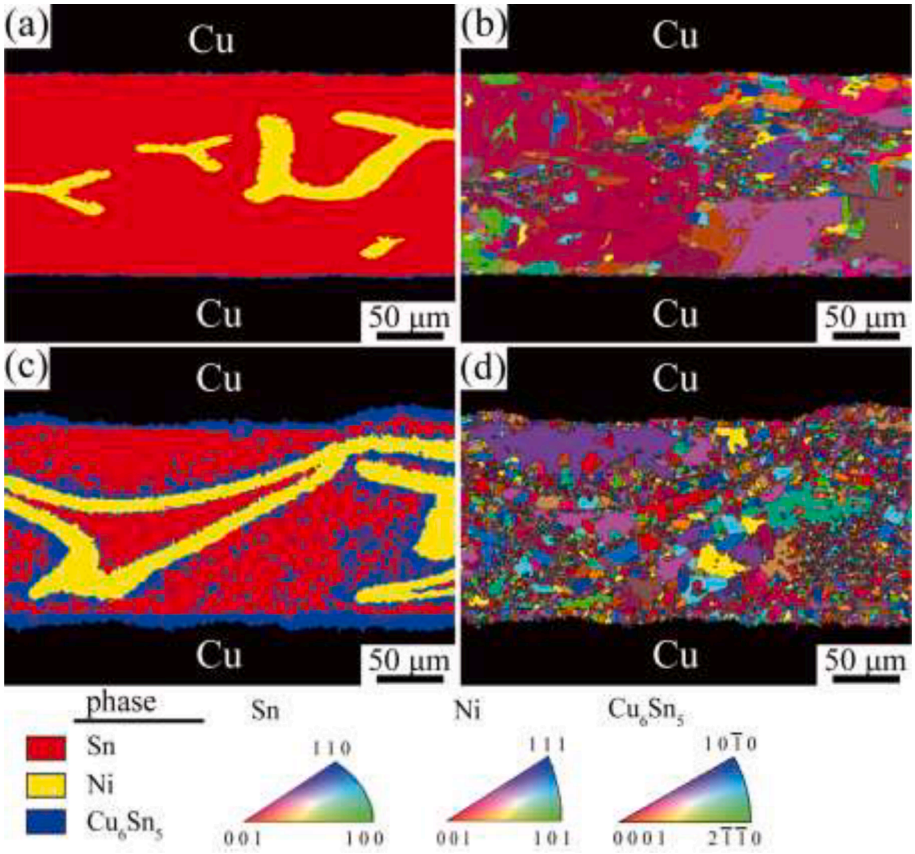

Fig. 7. EBSD analysis of Cu/Ni98-Sn/Cu joints ultrasonically soldered for different times. (a) (b) 5 s, (c) (d) 60 s.

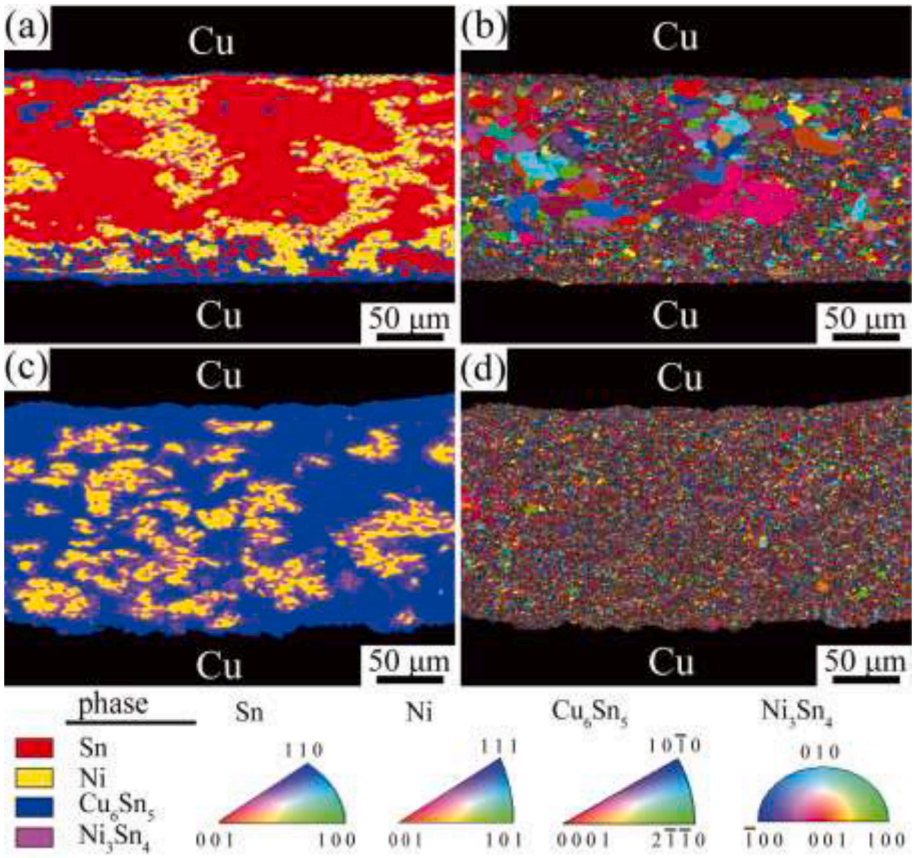

Fig. 8. EBSD analysis of Cu/Ni60-Sn/Cu joints ultrasonically soldered for different times. (a) (b) 5 s, (c) (d) 60 s.

effectively reduce the barrier effect and encourage the diffusion of Ni atoms from the Ni skeleton into Sn solder [12,30].

Furthermore, the Ni-Sn composite solders accelerate the metallurgical reaction and microstructure evolution during ultrasonic-assisted soldering. Firstly, Ni foam can create more solid/liquid interactions because of its large specific surface area and porous structure [22]. As a result, the Ni foam offers additional potential locations for the initiation of acoustic cavities [31]. Secondly, the pore diameters of Ni foam with 98 % and 60 % porosities are 200 μm and 50 μm, respectively, which are much bigger than the critical size of the cavitation effect generated in the molten alloys [15,32,33]. The creation of cavitation bubbles is therefore facilitated by the Ni-Sn composite solders. Thirdly, uneven $(Cu,Ni)_6Sn_5$ and $(Ni,Cu)_3Sn_4$ layers may effectively lower the energy barrier for the formation of acoustic cavities on the surfaces of Ni skeletons and Cu substrates, and they can also encourage cavitation bubbles to form at the solid/liquid interface.

By utilizing various Ni-Sn composite solders with ultrasonic assistance, the joints have varying IMCs. The $(Cu,Ni)_6Sn_5$ IMCs are produced on the surfaces of the Cu substrate and Ni skeleton in the Cu/Ni98-Sn/Cu joint, and Ni-Sn reactants are not present. This is mostly due to the fact that Cu atoms diffuse through Sn solder more quickly than Ni atoms do [34,35]. These findings are in line with those made public by Wang et al. [36] and Ji et al. [10]. There is a significant difference between the Cu joints utilizing Ni98-Sn and Ni60-Sn foils since several studies have shown that the Cu and Ni contents have a significant impact on the metallurgical processes in the Cu/Sn/Ni system [37–39]. In our previous study [40], the $(Cu, Ni)_6Sn_5$ and $(Ni, Cu)_3Sn_4$ phases transforming and grain refining process were studied. Results shown that a further solid-state diffusion reaction could induce the massive decomposition of $(Cu, Ni)_6Sn_5$ phase and the increase of $(Ni, Cu)_3Sn_4$ phase. Due to the growth of the $(Ni,Cu)_3Sn_4$ phase is mainly governed by the diffusion of Sn and Cu through grain boundary diffusion, the concentration gradient of Cu and Ni induced the massive nucleation of $(Ni,Cu)_3Sn_4$ IMC near the Ni skeleton surface. Hence, the $(Cu, Ni)_6Sn_5$ phase was massively transferred to the $(Ni, Cu)_3Sn_4$ phase accompanied by the refining of the $(Ni, Cu)_3Sn_4$ and $(Cu, Ni)_6Sn_5$ grains by prolonging the soldering time. Additionally, the Ni content of the Cu/Ni60-Sn/Cu joint is much larger than that of the Cu/Ni98-Sn/Cu joint, which results in $(Ni,Cu)_3Sn_4$ reactants on Ni skeletons rather than $(Cu,Ni)_6Sn_5$ reactants. Numerous Ni skeletons disintegrate when the soldering process is prolonged. The maximal solubility of Ni in $(Cu,Ni)_6Sn_5$ is 24 %, and when Ni concentration increases, $(Cu,Ni)_6Sn_5$ IMCs transforms to $(Ni,Cu)_3Sn_4$ IMCs [41,42]. As a result, The IMCs made with various Ni-Sn composite solder porosities vary widely.

Another noteworthy phenomenon is that only a very thin $(Ni, Cu)_3Sn_4$ layer exits on the surface of the Ni framework with the increase of soldering time in the Cu/Ni60-Sn/Cu joint. In the Cu/Ni98-Sn/Cu joint, the cracks existing on the granular $(Cu,Ni)_6Sn_5$ IMC is related to the cavitation effect. With the acoustic cavitation effect and continuous mechanical vibration, ultrasonic-assisted soldering can promote Ni atoms to spread out from Ni skeleton continuously, which results in the Ni content increasing in the $(Cu,Ni)_6Sn_5$ on Ni skeleton surface. As the Ni/Cu content changes, the $(Cu,Ni)_6Sn_5$ is more difficult to remain layered and breaks away from the Ni skeleton as small particles [43]. Meanwhile, the increasing and dissolution of Ni skeleton leads to $(Ni, Cu)_3Sn_4$ phase growing in the Cu/Ni60-Sn/Cu joint. The interfacial reaction layer transfers from a compact $(Ni,Cu)_3Sn_4$ IMC layer to a loose IMC layer as shown in Fig. 6 and Fig. 8 when ultrasonic-assisted soldering time from 5 s to 60 s. The $(Ni,Cu)_3Sn_4$ phase is not enough to remain layered as element content changes, and some break into small particles and disperse in the Sn matrix. Finally, the small particles and the refined $(Ni,Cu)_3Sn_4$ layer are squeezed between Ni skeletons, forming a loose structure. Under cavitation action and continuous mechanical vibration, the IMCs break off from Cu substrates and Ni

skeletons and dissociate to small particles in the soldering seam [44,45]. This explains that only a very thin $(Ni,Cu)_3Sn_4$ layer is on the surface of the Ni framework while the $(Cu,Ni)_6Sn_5$ phase is distributed throughout the Cu/Ni60-Sn/Cu joint.

Simultaneously, the Cu joints using Ni-Sn composite solder are contributed to grain refinement through ultrasonic-assisted soldering [46–48]. Many studies have shown that applying ultrasonic treatment can optimize the microstructure, refine the grain and improve the mechanical properties. Z. Xu etc. [47] obtained grain refinement of Al joints by applying cavitation and the grain refinement mechanism within narrow channels was proposed. The random cavitation induced nucleation of Sn was considered to be the main reason for grain refinement of the soldered joint in the narrow channel. The shear strength and hardness of the ultrasonically soldered joint increased obviously. A. Priyadarshi etc. [44] proved that the high pressure generated during the collapse of cavitation bubbles in liquid metal is one of the main driving forces for grain refinement. Application of ultrasound is shown to rapidly reduce intermetallic size and increase the number of potential nucleation sites. M. Dargusch etc. [46] evaluated the effect of cavitation, alloy chemistry, and fragmentation modes in microstructure refinement. During ultrasonic treatment, the refinement of grains and primary intermetallic compounds is realized by cavitation induced fragmentation mechanism. As ultrasonic time increasing, the IMCs gradually dissociated into refined particles and evenly distributed homogeneously in whole soldering seam under cavitation effect. Furthermore, Ni skeletons were dissolved and the IMCs were peeled off substrates into Sn solder. The Ni skeletons' large dissolution leads to Ni atoms concentration increases in the Sn solder, which accelerates the non-interfacial precipitation of Cu atoms. Hence, the nucleation of IMCs is increased and the IMCs' growing are promoted [49,50]. Meanwhile, the overgrowth of $(Cu,Ni)_6Sn_5$ grains is inhibited and the $(Cu,Ni)_6Sn_5$ and $(Ni,Cu)_3Sn_4$ IMCs are gradually transformed into fine particles, resulting in obvious grain refinement in the joints. Thus, the Ni-Sn composite solders are beneficial to the grain refinement through ultrasonic-assisted soldering.

In addition, due to the good strut of Ni foam, ultrasonic energy can transmit directly to the lower interface through Ni foam rather than only through liquid Sn solder, so the IMCs distribute more and more uniform under cavitation and vibration [51,52]. As ultrasonic time is prolongation, the proportion of liquid-phase in soldering seam decreases sharply, while the energy directly propagated by Ni foam is significantly reduced and the metallurgical reactions at the lower and upper interfaces tend to be consistent.

3.4. Shear strength and melting-point of joints

Shearing experiments were carried out to assess the mechanical characteristics of ultrasonic-assisted soldering joints by using various porosity Ni-Sn composite solders. The shear strength of Cu connections that were ultrasonically soldered with Ni98-Sn and Ni60-Sn foils throughout a range of soldering periods is shown in Fig. 9. The Cu/Ni98-Sn/Cu joint's shear strength rises and subsequently declines as soldering time is extended. But the Cu/Ni60-Sn/Cu joint's shear strength keeps rising. When employing Ni60-Sn foils during the same soldering process, a joint's shear strength is greater than when using Ni98-Sn foils. Cu/Ni98-Sn/Cu joints soldered for 30 s have a maximum shear strength of 36.9 MPa, while when soldered for 60 s, the shear strength drops slightly to 36.8 MPa. The shear strength of the Cu/Ni60-Sn/Cu joint, however, starts off at 77.5 MPa at 30 s and increases to 86.9 MPa at 60 s.

Fig. 10 shows the cross-section images of Cu joint after shear failure using different Ni-Sn composite solders. The fracture mechanism of joint using Ni98-Sn and Ni60-Sn foils are the same at the early stages. The joints soldered for 5 to 30 s mainly failed in the Sn solder interlayer as shown in Fig. 10(a)-(c) and Fig. 10(e)-(f). The $(Cu,Ni)_6Sn_5$ particles are observed and the fracture location is along the interface of $(Cu,Ni)_6Sn_5$ layer in the soldering seam. When the soldering time prolongs to 60 s,

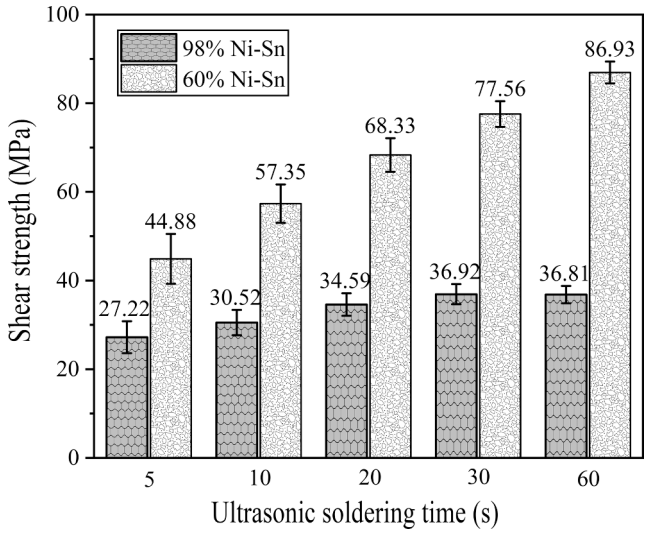

Fig. 9. Dependence of shear strength on ultrasonic soldering time for Cu/Ni-Sn/Cu joint.

Fig. 10(d) presents the Cu/Ni98-Sn/Cu joint mainly fails at the junction of $(Cu,Ni)_6Sn_5$ layer and Sn solder. However, Fig. 10(h) exhibits the Cu/Ni60-Sn/Cu joint breaks in $(Cu,Ni)_6Sn_5$ layer completely. The change of fracture position indicates that the IMCs and Ni skeletons play an important role in strengthening the joint. The $(Cu,Ni)_6Sn_5$ is a hard and brittle phase with a greatly different nature from Sn matrix. The obvious mismatch in hardness between these two phases causes the stress concentration and produces cracks at the junction. With the prolongation of soldering time, the IMCs gradually change from layered to granular shapes. The small granular reactants and Ni skeletons, uniformly distributed in the seam, hinder the crack propagation and improve the strength of joint effectively.

To further identify the melting-point of Cu joints, DSC characterizations were conducted. Fig. 11 shows the DSC and DTG curves of Cu joints with different composite solders ultrasonically soldered for 60 s. Two distinct types of composite solder joints first exhibited heat absorption, and then, as the temperature rose, they released a quantity of the heat that they had absorbed. The melting-point of Cu/Ni98-Sn/Cu joint is about 800 ℃ as shown in Fig. 11(a), which is around equal to the melting-point of Ni_3Sn_4 (794.5 ℃) [53]. The DTG pattern exhibits that the temperature of endothermic peak is 257.2 ℃, indicating that the phase transition is the reaction of Sn/Ni/Cu mainly occurred when Sn was melted. Fig. 11(b) presents that the melting point of Cu/Ni60-Sn/Cu joint is also around 800 ℃ and the temperature of endothermic peak is 618.7 ℃ which is almost similar to the phase transition temperature of Ni_3Sn_4 to Ni_3Sn_2 [54]. These substantiate the claim that the junctions fabricated using Ni foam reinforced Sn composite solders have a high melting point of 800°Celsius.

4. Conclusion

This effort included fabricating variable porosity Ni foam reinforced Sn composite solder foils to connect T2-Cu using ultrasonic-assisted soldering. The microstructure, grain morphology, and shear strength of Cu/Ni-Sn/Cu joints were studied in relation to foam porosity, ultrasonic vibration duration, and grain morphology. Following is a summary of the major conclusions:

(1) Two types of Ni-Sn composite solder foils that were both stronger than the total of the tensile strengths of the respective Ni foam reinforcement and the Sn matrix, greatly increased the tensile strengths of Sn solder.

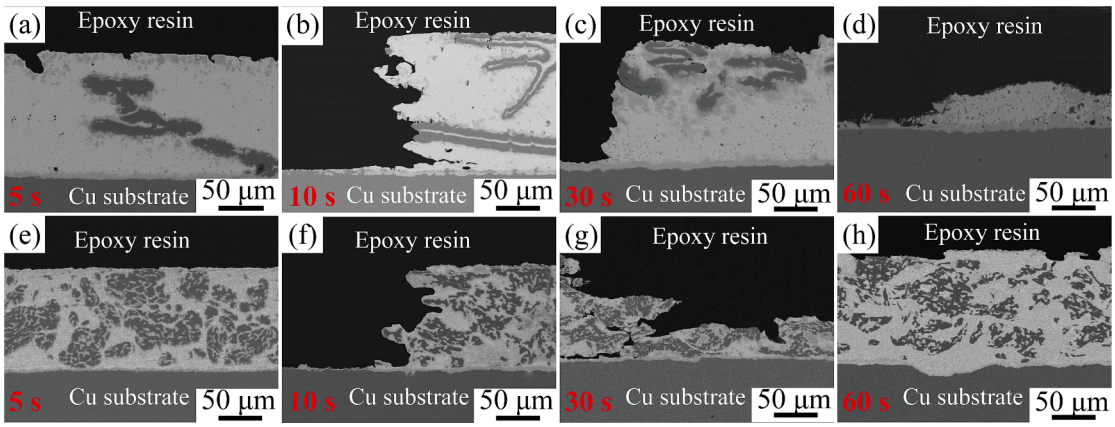

Fig. 10. Cross-section images of shear failed Cu joints ultrasonically soldered with (a-d) Ni98-Sn and (e-h) Ni60-Sn composite solder for 5, 10, 30, 60 s.

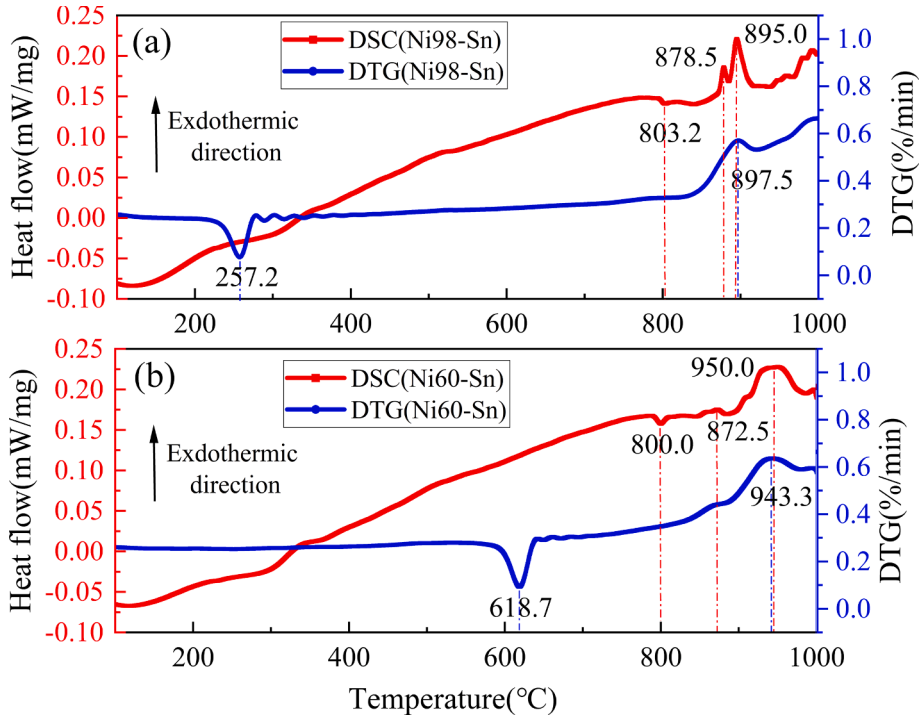

Fig. 11. DSC and DTG curves of Cu joints with different composite solders ultrasonically soldered for 60 s: (a) Ni98-Sn, (b) Ni60-Sn.

(2) The joints had different IMCs due to using various porosity Ni-Sn composite solders by ultrasonic-assisted soldering. Layered (Cu, Ni)$_6$Sn$_5$ and (Ni,Cu)$_3$Sn$_4$ phases both existed in Cu/Ni60-Sn/Cu joint while only (Cu,Ni)$_6$Sn$_5$ IMC grew in Cu/Ni98-Sn/Cu joint. The Ni skeletons were dissolved gradually, the IMCs peeled off substrates and dissociated into small particles evenly distributed homogeneously in whole soldering seams as ultrasonic-assisted soldering time increased.

(3) Ultrasonic-assisted soldering using different porosity Ni foam accelerated the metallurgical reaction and refined the IMCs grains. The Ni foam provided more solid/liquid interfaces and nucleation sites to promote the reaction rate under cavitation and the Ni atoms refined the IMCs grains.

(4) The Cu/Ni60-Sn/Cu joints had a greater shear strength than the Cu/Ni98-Sn/Cu joints, which had the greatest shear strength of 86.9 MPa after being ultrasonically soldered for 60 s and a high melting point of around 800 °C. The joints' strength was increased by the homogeneously dispersed granular IMCs and Ni skeletons, which prevented fracture propagation.

CRediT authorship contribution statement

Huang He: Investigation, Data curation, Formal analysis, Writing – original draft. **Lizhi Song:** Data curation. **Haitao Gao:** Resources, Funding acquisition. **Yong Xiao:** Conceptualization, Methodology, Resources, Writing – review & editing, Supervision. **Yi Cao:** Resources, Writing – review & editing.

Declaration of Competing Interest

The authors declare that they have no known competing financial interests or personal relationships that could have appeared to influence the work reported in this paper.

Data availability

Data will be made available on request.

Acknowledgments

Dr. Huang He is grateful to the Brazing Research Group in the Guangdong Provincial Key Laboratory of Advanced Welding Technology. Dr. Haitao Gao gratefully acknowledges the GDAS' Project of Science and Technology Development [2022GDASZH-2022010109].

References

[1] J.W. Ronnie Teo, Y.F. Sun, Spalling behavior of interfacial intermetallic compounds in Pb-free solder joints subjected to temperature cycling loading, Acta Mater. 56 (2) (2008) 242–249.
[2] K.J. Zeng, K.N. Tu, Six cases of reliability study of Pb-free solder joints in electronic packaging technology, Mater. Sci. Eng., R 38 (2) (2002) 55–105.
[3] C. Buttay, D. Planson, B. Allard, D. Bergogne, P. Bevilacqua, C. Joubert, M. Lazar, C. Martin, H. Morel, D. Tournier, State of the art of high temperature power electronics, Mater. Sci. Eng., B 176 (4) (2011) 283–288.
[4] L. Sun, M. Chen, L. Zhang, P. He, L. Xie, Recent progress in SLID bonding in novel 3D-IC technologies, J. Alloys Compd. 818 (2020), 152825.
[5] L. Zhang, Z.Q. Liu, S.W. Chen, Y.D. Wang, W.M. Long, Y.H. Guo, S.Q. Wang, G. Ye, W.Y. Liu, Materials, processing and reliability of low temperature bonding in 3D chip stacking, J. Alloys Compd. 750 (2018) 980–995.
[6] H. He, S. Huang, Y. Ye, Y. Xiao, Z. Zhang, M. Li, R. Goodall, Microstructure and mechanical properties of Cu joints soldered with a Sn-based composite solder, reinforced by metal foam, J. Alloys Compd. 845 (2020), 156240.
[7] Y. Xiao, Z. Song, S. Li, D. Li, Z. Zhang, M. Li, R. Goodall, Bonding and strengthening mechanism of ultrasonically soldered 7075 Al joint using Ni foam/Sn composite solder foil, Mater. Sci. Eng., A 791 (2020).
[8] D.S. Kharitonov, A.A. Kasach, D.S. Sergievich, A. Wrzesinska, I. Bobowska, K. Darowicki, A. Zielinski, J. Ryl, Kurilo, II, Ultrasonic-assisted electrodeposition of Cu-Sn-TiO_2 nanocomposite coatings with enhanced antibacterial activity, Ultrason. Sonochem. 75 (2021), 105593.
[9] Z.L. Li, H.J. Dong, X.G. Song, H.Y. Zhao, H. Tian, J.H. Liu, J.C. Feng, J.C. Yan, Homogeneous (Cu, Ni)$_6$Sn$_5$ intermetallic compound joints rapidly formed in asymmetrical Ni/Sn/Cu system using ultrasound-induced transient liquid phase soldering process, Ultrason. Sonochem. 42 (2018) 403–410.
[10] H. Ji, Y. Qiao, M. Li, Rapid formation of intermetallic joints through ultrasonic-assisted die bonding with Sn–0.7Cu solder for high temperature packaging application, Scripta Mater. 110 (2016) 19–23.
[11] W. Zhang, Y. Cao, J. Huang, W. Zhao, X. Liu, M. Li, H. Ji, Ultrasonic-accelerated metallurgical reaction of Sn/Ni composite solder: Principle, kinetics, microstructure, and joint properties, Ultrason. Sonochem. 66 (2020), 105090.
[12] Z.L. Li, H.J. Dong, X. Song, H.Y. Zhao, J.C. Feng, J.H. Liu, H. Tian, S.J. Wang, Rapid formation of Ni3Sn4 joints for die attachment of SiC-based high temperature power devices using ultrasound-induced transient liquid phase bonding process, Ultrason. Sonochem. 36 (2017) 420–426.
[13] G.S.B. Lebon, I. Tzanakis, K. Pericleous, D.G. Eskin, P.S. Grant, Ultrasonic liquid metal processing: The essential role of cavitation bubbles in controlling acoustic streaming, Ultrason. Sonochem. 55 (2019) 243–255.
[14] W.L. Niu, Y. Xiao, C. Wan, D. Li, H.Q. Fu, H. He, Ultrasonic bonding of 2024 Al alloy using Ni foam/Sn composite solder at ambient temperature, Mater. Sci. Eng., A 771 (2020), 138663.
[15] R. Pflieger, S.I. Nikitenko, C. Cairós, R. Mettin, Characterization of Cavitation Bubbles and Sonoluminescence, Springer Nature, 2019.
[16] M. Ashokkumar, J. Lee, S. Kentish, F. Grieser, Bubbles in an acoustic field: an overview, Ultrason. Sonochem. 14 (4) (2007) 470–475.
[17] W.W. Xu, I. Tzanakis, P. Srirangam, W.U. Mirihanage, D.G. Eskin, A.J. Bodey, P. D. Lee, Synchrotron quantification of ultrasound cavitation and bubble dynamics in Al-10Cu melts, Ultrason. Sonochem. 31 (2016) 355–361.
[18] D.G. Eskin, I. Tzanakis, F. Wang, G.S.B. Lebon, T. Subroto, K. Pericleous, J. Mi, Fundamental studies of ultrasonic melt processing, Ultrason. Sonochem. 52 (2019) 455–467.
[19] Z.L. Li, H. Tian, H.J. Dong, X.J. Guo, X.G. Song, H.Y. Zhao, J.C. Feng, The nucleation-controlled intermetallic grain refinement of Cu-Sn solid-liquid interdiffusion wafer bonding joints induced by addition of Ni particles, Scripta Mater. 156 (2018) 1–5.
[20] X.D. Zhang, X.W. Hu, X.X. Jiang, Y.L. Li, Effect of Ni addition to the Cu substrate on the interfacial reaction and IMC growth with Sn3.0Ag0.5Cu solder, Appl. Phys. A 124 (4) (2018) 315.
[21] A. Wierzbicka-Miernik, J. Wojewoda-Budka, K. Miernik, L. Litynska-Dobrzynska, N. Schell, Characteristics of intermetallic phases in Cu/(Sn, Ni) diffusion couples annealed at 220 °C, J. Alloys Compd. 693 (2017) 1102–1108.
[22] Y. Xiao, Q. Wang, L. Wang, X. Zeng, M. Li, Z. Wang, X. Zhang, X. Zhu, Ultrasonic soldering of Cu alloy using Ni foam/Sn composite interlayer, Ultrason. Sonochem. 45 (2018) 223–230.
[23] Y. Xiao, S. Li, Z. Wang, Y. Xiao, Z. Song, Y. Mao, M. Li, Microstructure and mechanical properties of 7075-Al alloy joint ultrasonically soldered with Ni foam/Sn composite solder, Mater. Sci. Eng., A 729 (2018) 241–248.
[24] H. Ji, J. Zhou, M. Liang, H. Lu, M. Li, Ultra-low temperature sintering of Cu@Ag core-shell nanoparticle paste by ultrasonic in air for high-temperature power device packaging, Ultrason. Sonochem. 41 (2018) 375–381.
[25] Y.T. Didenko, W.B. McNamara, K.S. Suslick, Hot spot conditions during cavitation in water, J. Am. Chem. Soc. 121 (24) (1999) 5817–5818.
[26] K.S. Suslick, D.A. Hammerton, R.E. Cline, The Sonochemical Hot Spot, J. Am. Chem. Soc. 108 (18) (1986) 5641–5642.
[27] E.B. Flint, K.S. Suslick, The temperature of cavitation, Science 253 (5026) (1991) 1397–1399.
[28] R. Pflieger, G. Audiger, S.I. Nikitenko, M. Ashokkumar, Impact of bubble coalescence in the determination of bubble sizes using a pulsed US technique: Part 2 - Effect of the nature of saturating gas, Ultrason. Sonochem. 73 (2021), 105537.
[29] T. Xu, X. Hu, Y. Li, X. Jiang, X. Yu, Significant Inhibition of IMCs Growth between an Electroless Ni-W-P Metallization and SAC305 Solder During Soldering and Aging, Journal of Wuhan University of Technology-Mater Sci. Ed. 34 (1) (2019) 165–175.
[30] M. Dular, O.C. Delgosha, M. Petkovsek, Observations of cavitation erosion pit formation, Ultrason. Sonochem. 20 (4) (2013) 1113–1120.
[31] D.G. Shchukin, E.V. Skorb, V. Belova, H. Mohwald, Ultrasonic Cavitation at Solid Surfaces, Adv. Mater. 23 (17) (2011) 1922–1934.
[32] A. Brotchie, F. Grieser, M. Ashokkumar, Effect of Power and Frequency on Bubble-Size Distributions in Acoustic Cavitation, Phys. Rev. Lett. 102 (8) (2009), 084302.
[33] R. Pflieger, J. Bertolo, L. Gravier, S.I. Nikitenko, M. Ashokkumar, Impact of bubble coalescence in the determination of bubble sizes using a pulsed US technique: Part 1 - Argon bubbles in water, Ultrason. Sonochem. 73 (2021), 105532.
[34] H.J. Dong, Z.L. Li, X.G. Song, H.Y. Zhao, H. Tian, J.H. Liu, J.C. Yan, Grain morphology evolution and mechanical strength change of intermetallic joints formed in Ni/Sn/Cu system with variety of transient liquid phase soldering temperatures, Mater. Sci. Eng., A 705 (2017) 360–365.
[35] V.A. Baheti, S. Kashyap, P. Kumar, K. Chattopadhyay, A. Paul, Solid–state diffusion–controlled growth of the intermediate phases from room temperature to an elevated temperature in the Cu–Sn and the Ni–Sn systems, J. Alloys Compd. 727 (2017) 832–840.
[36] C. Wang, S. Chen, Sn–0.7wt.%Cu/Ni interfacial reactions at 250°C, Acta Mater. 54 (1) (2006) 247–253.
[37] S.C. Yang, C.C. Chang, M.H. Tsai, C.R. Kao, Effect of Cu concentration, solder volume, and temperature on the reaction between SnAgCu solders and Ni, J. Alloys Compd. 499 (2) (2010) 149–153.
[38] Y.S. Huang, H.Y. Hsiao, C. Chen, K.N. Tu, The effect of a concentration gradient on interfacial reactions in microbumps of Ni/SnAg/Cu during liquid-state soldering, Scripta Mater. 66 (10) (2012) 741–744.
[39] V.A. Baheti, S. Islam, P. Kumar, R. Ravi, R. Narayanan, D. Hongqun, V. Vuorinen, T. Laurila, A. Paul, Effect of Ni content on the diffusion-controlled growth of the product phases in the Cu(Ni)–Sn system, Philos. Mag. 96 (1) (2015) 15–30.
[40] H. He, S. Huang, Y. Xiao, R. Goodall, Diffusion reaction-induced microstructure and strength evolution of Cu joints bonded with Sn-based solder containing Ni-foam, Mater. Lett. 281 (2020).
[41] C.Y. Li, Phase distribution and phase analysis in Cu_6Sn_5, Ni_3Sn_4, and the Sn-rich corner in the ternary Sn-Cu-Ni isotherm at 240°C, J. Electron. Mater. 35 (2006).
[42] H.M. Henao, C.S. Chu, J.P. Solis, K. Nogita, Experimental determination of the Sn-Cu-Ni phase diagram for Pb-free solder applications, Metall. Mater. Trans. B 50 (1) (2019) 502–516.
[43] J. Yoon, B. Noh, S. Jung, Comparative study of ENIG and ENEPIG as surface finishes for a Sn-Ag-Cu solder joint, J. Electron. Mater. 40 (9) (2011) 1950–1955.
[44] A. Priyadarshi, M. Khavari, T. Subroto, M. Conte, P. Prentice, K. Pericleous, D. Eskin, J. Durodola, I. Tzanakis, On the governing fragmentation mechanism of primary intermetallics by induced cavitation, Ultrason. Sonochem. 70 (2021), 105260.
[45] A. Priyadarshi, M. Khavari, S. Bin Shahrani, T. Subroto, L.A. Yusuf, M. Conte, P. Prentice, K. Pericleous, D. Eskin, I. Tzanakis, In-situ observations and acoustic measurements upon fragmentation of free-floating intermetallics under ultrasonic cavitation in water, Ultrason. Sonochem. 80 (2021), 105820.
[46] N. Balasubramani, J. Venezuela, N. Yang, G. Wang, D. StJohn, M. Dargusch, An overview and critical assessment of the mechanisms of microstructural refinement during ultrasonic solidification of metals, Ultrason. Sonochem. 89 (2022), 106151.
[47] Z. Li, Z. Xu, D. Zhao, X. Liu, J. Yan, Grain refinement caused by intensified cavitation within narrow channel and its improvement to ultrasonically soldered Al joint property, Ultrason. Sonochem. 60 (2020), 104786.
[48] H. Huang, L. Qin, H. Tang, D. Shu, W. Yan, B. Sun, J. Mi, Ultrasound cavitation induced nucleation in metal solidification: An analytical model and validation by real-time experiments, Ultrason. Sonochem. 80 (2021), 105832.
[49] F. Wang, D. Eskin, J. Mi, C. Wang, B. Koe, A. King, C. Reinhard, T. Connolley, A synchrotron X-radiography study of the fragmentation and refinement of primary intermetallic particles in an Al-35 Cu alloy induced by ultrasonic melt processing, Acta Mater. 141 (2017) 142–153.
[50] B. Wang, D. Tan, T.L. Lee, J.C. Khong, F. Wang, D.G. Eskin, T. Connolley, K. Fezzaa, J. Mi, Ultrafast synchrotron X-ray imaging studies of microstructure fragmentation in solidification under ultrasound, Acta Mater. 144 (2018) 505–515.
[51] Z. Li, M. Li, Y. Xiao, C. Wang, Ultrarapid formation of homogeneous Cu_6Sn_5 and Cu_3Sn intermetallic compound joints at room temperature using ultrasonic waves, Ultrason. Sonochem. 21 (3) (2014) 924–929.

[52] Y. Shen, L. Zhang, Y. Wu, W. Chen, The role of the bubble-bubble interaction on radial pulsations of bubbles, Ultrason. Sonochem. 73 (2021), 105535.
[53] C. Schmetterer, H. Flandorfer, K.W. Richter, U. Saeed, M. Kauffman, P. Roussel, H. Ipser, A new investigation of the system Ni-Sn, Intermetallics 15 (7) (2007) 869–884.
[54] W.F. Gale, T.C. Totemeier, Smithells Metals Reference Book (Eighth Edition) (2004).